PLOS GENETICS

RESEARCH ARTICLE

Miro-dependent mitochondrial pool of CENP-F and its farnesylated C-terminal domain are dispensable for normal development in mice

Martin Peterka[1,2], **Benoît Kornmann**[1¤*]

1 Institute of Biochemistry, ETH Zurich, Zürich, Switzerland, **2** Molecular Life Science Program, Zurich Life-Science Graduate School, Zürich, Switzerland

¤ Current address: Department of Biochemistry, University of Oxford, Oxford, United Kingdom.
* benoit.kornmann@bioch.ox.ac.uk

Citation: Peterka M, Kornmann B (2019) Miro-dependent mitochondrial pool of CENP-F and its farnesylated C-terminal domain are dispensable for normal development in mice. PLoS Genet 15(3): e1008050. https://doi.org/10.1371/journal.pgen.1008050

Editor: Aleksandra Trifunovic, University of Cologne, GERMANY

Received: September 14, 2018

Accepted: February 27, 2019

Published: March 11, 2019

Data Availability Statement: All relevant data are within the manuscript and its Supporting Information files.

Funding: This work was funded by grants from the ERC (337906-Orga-Net) and the Swiss National Science Foundation (PP00P3_13365) to BK. The funders had no role in study design, data collection and analysis, decision to publish, or preparation of the manuscript.

Competing interests: The authors have declared that no competing interests exist.

Abstract

CENP-F is a large, microtubule-binding protein that regulates multiple cellular processes including chromosome segregation and mitochondrial trafficking at cytokinesis. This multiplicity of functions is mediated through the binding of various partners, like Bub1 at the kinetochore and Miro at mitochondria. Due to the multifunctionality of CENP-F, the cellular phenotypes observed upon its depletion are difficult to interpret and there is a need to genetically separate its different functions by preventing binding to selected partners. Here we engineer a CENP-F point-mutant that is deficient in Miro binding and thus is unable to localize to mitochondria, but retains other localizations. We introduce this mutation in cultured human cells using CRISPR/Cas9 system and show it causes a defect in mitochondrial spreading similar to that observed upon Miro depletion. We further create a mouse model carrying this CENP-F variant, as well as truncated CENP-F mutants lacking the farnesylated C-terminus of the protein. Importantly, one of these truncations leads to ~80% downregulation of CENP-F expression. We observe that, despite the phenotypes apparent in cultured cells, mutant mice develop normally. Taken together, these mice will serve as important models to study CENP-F biology at organismal level. In addition, because truncations of CENP-F in humans cause a lethal disease termed Strømme syndrome, they might also be relevant disease models.

Author summary

CENP-F is a poorly characterized multifunctional regulator of metazoan cell division involved in chromosome segregation and mitochondrial dynamics. The physiological importance of CENP-F in both of these processes is not firmly established and numerous conflicting reports exist regarding its function in mitosis. Here we set out to investigate the function of CENP-F *in vivo* by CRISPR-mediated mutagenesis in mice where we specifically disrupt different domains of CENP-F important for mitosis and mitochondrial regulation. Surprisingly, contrasting to reported phenotypes in cultured cells, mutant animals display no obvious phenotypes. This argues against CENP-F being a major player in

mammalian cell division and suggest context-specific roles of this protein. Importantly, in humans, truncations of CENP-F as small as 20 amino acids have recently emerged as a cause of human disease termed Strømme syndrome. Truncations in these mice might yield information relevant to the understanding of this disease and biology of CENP-F.

Introduction

CENP-F is a large coiled coil protein that was originally found as a kinetochore binding protein [1]. It is apparent from recent work that CENP-F also functions in mitochondrial transport, nuclear envelope breakdown, microtubule polymerization, and transcriptional regulation via its interactions with the retinoblastoma protein and ATF4 [2–5]. Despite its multitude of subcellular localizations and binding partners, the physiological function of CENP-F remains poorly defined. To our knowledge, the only known phenotype observed upon CENP-F loss is dilated cardiomyopathy described in a heart-specific conditional knockout mice [6].

In humans, aberrant expression of CENP-F has been implicated in prostate cancer [7]. In addition, mutations in CENP-F are known to cause Strømme syndrome, a rare autosomal recessive disorder characterized by microcephaly, intestinal atresia and other ciliopathy phenotypes [8–10].

Both the expression level and subcellular localization of CENP-F are regulated in a cell-cycle-dependent manner. Undetectable in G1, CENP-F accumulates in the nucleus during S/G2. At this stage, a fraction of CENP-F is exported and recruited to the outer nuclear envelope (NE) where it interacts with the nucleoporin Nup133 and participates in the recruitment of dynein [11]. Subsequently in prometaphase, CENP-F relocates to kinetochores [1]. The molecular mechanism of CENP-F kinetochore binding has been studied in great detail [12–14]. CENP-F is targeted to the outer kinetochore via a KT-core domain (residues 2792 to 2887, Fig 1A) via synergistic action of Bub1 kinase and the kinesin Cenp-E [12, 14]. In turn, CENP-F recruits Ndel1/Nde1/Lis1/Dynein complex necessary for chromosome segregation. In addition, a recent report showed that CENP-F is a receptor for ATR at the kinetochore and therefore an upstream trigger of the ATR-Chk1-Aurora B pathway necessary for the proper segregation of chromosomes [15]. Nevertheless, the relevance of CENP-F at the kinetochore is controversial. Numerous studies reported defects in chromosome segregation and/or cell-cycle progression upon depletion of CENP-F or inhibition of its kinetochore localization [5, 16–21]. While conflicting reports showed no defects in mitosis upon CENP-F loss [13, 22–24].

After exerting its function at kinetochores in mitosis, CENP-F is recruited in cytokinesis to the outer mitochondrial membrane by the atypical GTPases Miro1 and Miro2 [4]. The Miro-binding domain is highly conserved and located near the C-terminus (2977–3020, Fig 1A) of CENP-F. Mechanistically, CENP-F appears to be linking mitochondria with the growing microtubule tips and harnessing the force generated by microtubule growth [4, 25]. This process helps the mitochondrial network to properly distribute throughout the cytoplasm during cytokinesis. Upon CENP-F depletion, mitochondria fail to spread to the cell periphery and remain clumped in the perinuclear area, phenocopying Miro depletion. Of note, a fraction of CENP-F is localized on mitochondria also in G2 [4, 25]. The physiological function of the mitochondrial fraction of CENP-F remains unknown.

Bracketing its coiled-coils, CENP-F harbors two microtubule-binding domains of unknown functions at both termini of the protein [5]. Both domains have microtubule tip-tracking properties and a unique ability to transport cargo *in vitro* continuously with both growing and

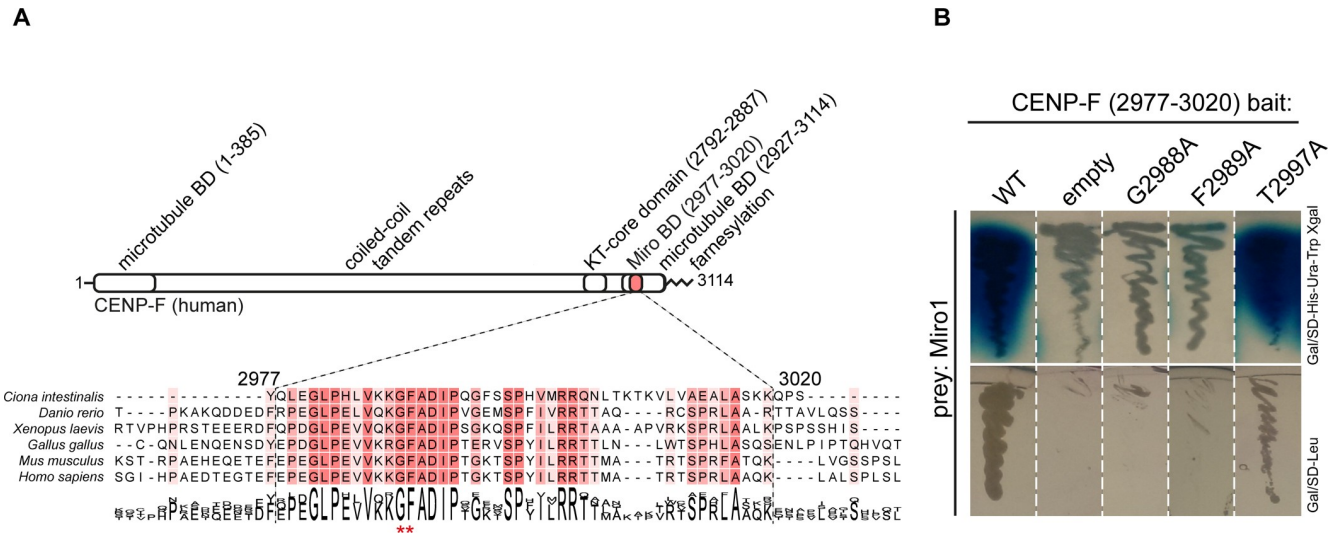

Fig 1. Disruption of CENP-F-Miro complex by single point mutations in CENP-F. A) Domain organization of CENP-F and alignment of Miro-binding domains from chordates. Red asterisks mark residues G2988A and F2989A essential for Miro binding. **B)** Yeast two-hybrid assay using strains containing denoted plasmids. Top row: X-gal overlay assay, bottom row: growth assay on leucine dropout medium.

https://doi.org/10.1371/journal.pgen.1008050.g001

shrinking microtubules, with the C-terminus being a more robust mediator of these movements [25, 26]. In cells, full-length CENP-F can track growing microtubule tips [25]. These properties of CENP-F further substantiate its potential role in supporting microtubule tip-mediated transport of cellular cargoes such as chromosomes and mitochondria.

Additionally, CENP-F contains a CaaX motif, which is farnesylated [27]. However, functional consequences of CENP-F farnesylation have been debated. The CaaX motif of CENP-F has been proposed to be necessary for its kinetochore and NE localization [28, 29]. Moreover, inhibition of CENP-F farnesylation led to defective degradation of the protein and delayed G2/M progression in cancer cells [28, 30]. On the other hand, more recent studies showed only a mild or no effect of farnesylation on CENP-F kinetochore localization [31, 32]. Thus, the function and physiological relevance of CENP-F farnesylation remain unresolved.

The plethora of interacting partners and cellular localizations make studying CENP-F a challenge, and the cellular phenotypes observed upon CENP-F depletion are difficult to interpret due to the multifunctionality of the protein.

Here, using a single point mutation within the Miro-binding region of CENP-F, we genetically separated the mitochondrial function from other functions of CENP-F. We used CRISPR/Cas9-mediated mutagenesis to introduce this mutation in human cells. Furthermore, to gain a physiological insight into mitochondrial function of CENP-F, we engineered a similar mutation in mice. Moreover, as a by-product of CRISPR/Cas9-mediated engineering, we generated animals bearing truncated CENP-F alleles lacking the last two exons of CENP-F, which encode the C-terminal microtubule-binding domain and the farnesylation motif. In addition to the loss of the C-terminal domain, one of the mutations resulted in approximately 80% decrease of overall CENP-F expression. Strikingly, despite the plethora of functions attributed to CENP-F, these mice are viable and fertile, and do not display any obvious phenotype. These different mouse models will be instrumental to systematically study the multiple functions of CENP-F in different tissues and under different physiological or pathological conditions.

Results

We have previously mapped the Miro1/2-binding domain in CENP-F to a C-terminal region spanning residues 2977–3020 of human CENP-F, which is among the best conserved parts of the protein (Fig 1A) [4]. Here, in order to specifically disrupt the interaction between CENP-F and Miro, we used alanine-scanning mutagenesis in the yeast two-hybrid assay and found that alanine substitution of the highly conserved CENP-F residue G2988 or F2989 completely abrogated Miro binding. On the other hand, alanine substitution of the non-conserved residue T2997 did not influence Miro1 binding in this assay (Fig 1B). The Miro-binding domain of CENP-F partially overlaps with a sequence motif involved in binding the retinoblastoma (RB) protein [33]. We thus wondered whether the F2989A mutation also affected this interaction. We could not however assess this point since we were not able to detect a yeast two-hybrid interaction between neither full length RB nor $RB^{301\text{-}918}$ (previously shown to be functional in yeast two hybrid assay [34]) and wild type CENP-F (S1A and S1B Fig).

Therefore, the interaction between CENP-F and Miro in yeast two-hybrid assay can be disrupted by a single point mutation, offering an opportunity to genetically separate the mitochondrial from other functions of this large multifaceted protein.

To characterize the properties of $CENP\text{-}F^{F2989A}$ in human cells, we engineered the F2989A substitution into the endogenous *CENP-F* locus using CRISPR/Cas9-mediated genome editing (Fig 2A, 2B and 2C). We performed the substitution in human osteosarcoma cell line U2OS, which displays high levels of Miro-dependent mitochondrial recruitment of CENP-F in S/G2 and cytokinesis [4].

Our approach using co-electroporation of Cas9 RNP complexes and a 130nt single-stranded DNA homology-directed repair template yielded homozygous F2989A substitution in one out of 43 clones screened. 14 additional clones were heterozygous. This relatively high ratio of heterozygous versus homozygous modifications might be a consequence of polyploidy of U2OS cells [35]. To obtain additional homozygous clones for robust analysis, we re-targeted *CENP-F* in one heterozygous clone obtained in the first round of targeting. In this second round, 8 out of 26 clones were homozygous for $CENP\text{-}F^{F2989A}$.

$CENP\text{-}F^{F2989A}$ recapitulated the cell-cycle-dependent expression and localization patterns of the WT CENP-F. It was well expressed (Fig 2D), accumulated in the nucleus during the S/G2 (Fig 3A), localized at the midbody in cytokinesis (Fig 3A), localized to the nuclear envelope in early prophase (Fig 3B) and to the kinetochores in mitosis (Fig 3C). However, while WT CENP-F could be seen accumulated on mitochondria in S/G2 and cytokinetic cells as previously described, $CENP\text{-}F^{F2989A}$ remained diffuse in the cytosol throughout these cell-cycle phases (Fig 3A). This phenotype was robust as it was also observed in another independently obtained mutant clone (S1D Fig). Taken together, these results indicate that F2989A mutation in CENP-F solely affects the mitochondrial localization of the protein.

We have previously shown that siRNA-mediated depletion of CENP-F leads to defective distribution of the mitochondrial network throughout the cytoplasm. This defect most likely originates in cytokinesis during which CENP-F-depleted cells fail to redistribute mitochondria to the cell periphery [4]. Yet, this phenotype might have been a side effect of total CENP-F depletion, rather than a direct result of the absence of the mitochondrial pool of CENP-F. The $CENP\text{-}F^{F2989A}$ cells thus presented a unique opportunity to distinguish these two possibilities. $CENP\text{-}F^{F2989A}$ cells recapitulated the mitochondrial phenotypes of global CENP-F or Miro depletion in cytokinesis, displaying typical "clumped" mitochondria that failed to extend to the cell periphery (Fig 4A). Moreover, in interphase, mutant cells often displayed similar phenotype. This was not due to a failure of cell spreading, as bright-field imaging did not reveal aberrant cell shapes (Fig 4B). To quantify mitochondrial clumping in $CENP\text{-}F^{F2989A}$ cells, we

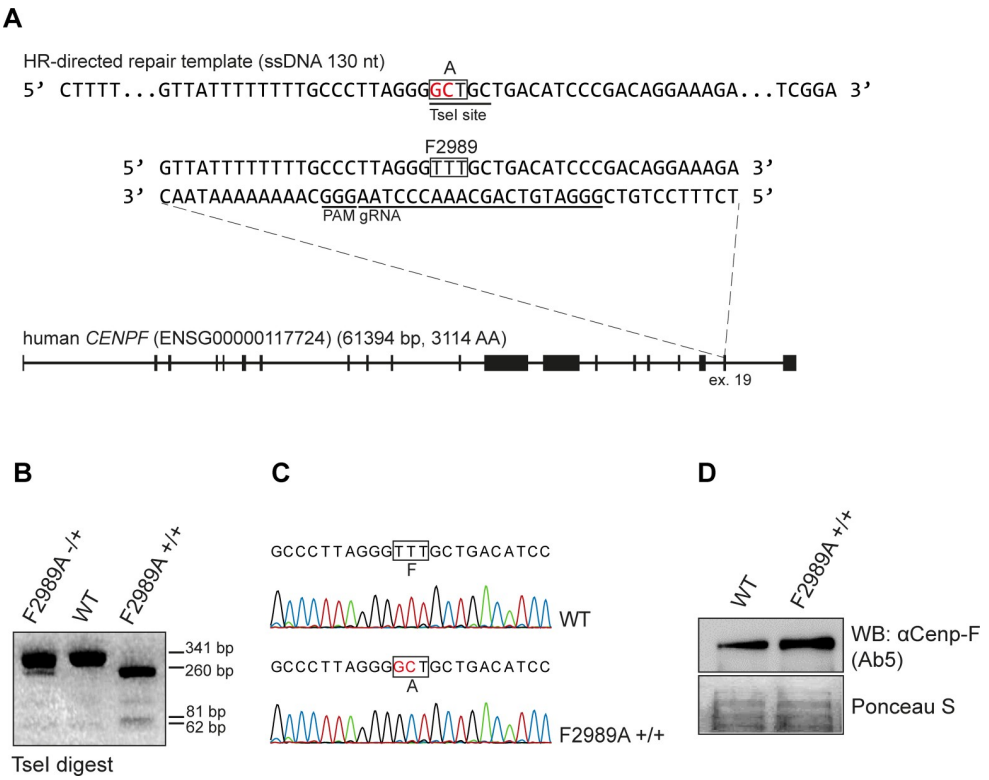

Fig 2. Introduction of the F2989A *CENP-F* mutation in human cells. A) Targeting strategy to engineer F2989A mutation in CENP-F using CRISPR/Cas9 in U2OS cells. 2nt substitution includes TseI restriction site to facilitate screening for correctly modified clones. **B)** TseI digested PCR products of the targeted *CENP-F* locus from WT, heterozygous and homozygous $CenpF^{F2989A}$ U2OS cells. The expected restriction fragment sizes are 341 and 62 bp for the *wild type* allele and 260, 81 and 62 bp for the *F2989A* allele. **C)** Sequencing electropherograms of the targeted *CENP-F* area from WT and homozygous $CenpF^{F2989A}$ U2OS cells. **D)** Western blot on WT or $CenpF^{F2989A}$ U2OS cells using Ab5 antibody.

https://doi.org/10.1371/journal.pgen.1008050.g002

used an informatics approach that we have developed previously and that computes the "moment of inertia" of the mitochondrial network. This analysis measures the distance of each mitochondrial pixel to the cell's center of mass, and thus, reflects the spreading of the mitochondrial network [4]. Two independent clones (cl.1 and cl.2) bearing the homozygous *CENP-F*^{F2989A} mutation displayed a reduction in mitochondrial spreading, similar to what has been observed upon complete depletion of Miro or CENP-F (Fig 4C, and [4]). Therefore, the Miro-recruited mitochondrial fraction of CENP-F ensures that mitochondria are properly distributed throughout the cytoplasm in cytokinesis. Defective mitochondrial distribution in these cells however, did not lead to obvious defects in mitochondrial function as neither basal respiration, coupled respiration, nor extracellular acidification rate were detectably affected in these cells (Fig 4D).

To gain insight into the physiological function of mitochondrial CENP-F at the organismal level, we turned to genome editing in mice to mutate the conserved F2872 residue (cognate to human F2989) to alanine. For this purpose, we used pronuclear microinjection of preformed Cas9-gRNA complexes together with a single-stranded 130 bp homology-directed repair template (Fig 5A). In two microinjection sessions, we obtained 4 (20%) founders bearing heterozygous modification of the targeted F2872. These mutations were heritable, as crossing two heterozygous founders resulted in homozygous F1 mutant pups in expected Mendelian ratios

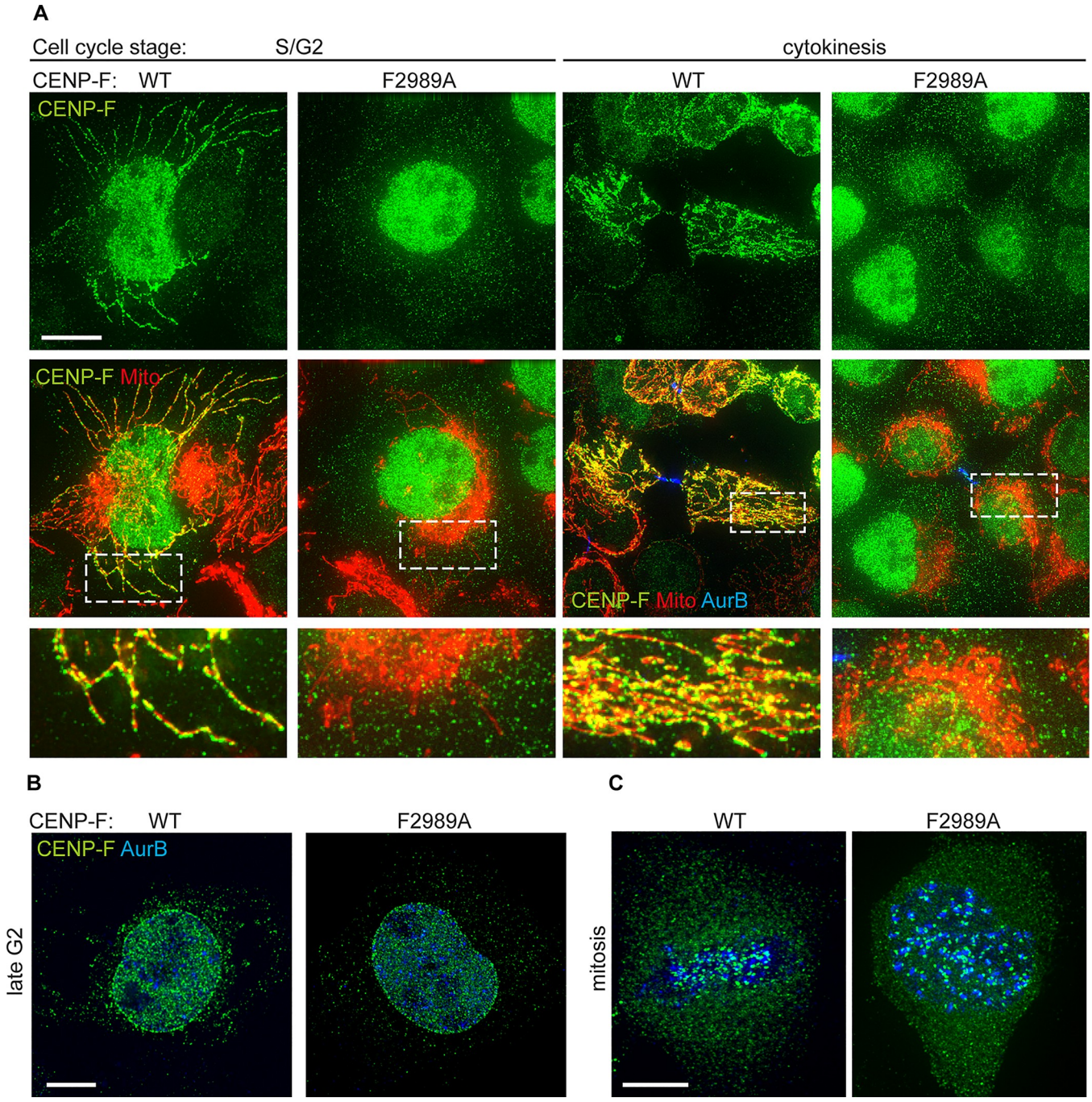

Fig 3. *F2989A* disrupts CENP-F localization at mitochondria in human cells without affecting its localization at the nuclear envelope and kinetochores. **A)** Immunofluorescence of mitochondrial marker-expressing (mtBFP) S/G2 or cytokinetic *CENP-F*^{WT} or *CENP-F*^{F2989A} cells using a CENP-F antibody (Ab5) **B)** Immunofluorescence of *CENP-F*^{WT} *or CENP-F*^{F2989A} U2OS cells in late G2 using CENP-F (Ab5) and AuroraB antibodies. **C)** Immunofluorescence of *CENP-F*^{WT} or *CENP-F*^{F2989A} U2OS cells in mitosis using CENP-F (Ab5) and AuroraB antibodies. Scale bars 5 μm.

https://doi.org/10.1371/journal.pgen.1008050.g003

(Fig 5B, Table 1). These homozygous animals (Fig 5C) were viable, fertile and reached adulthood without any apparent phenotype.

We used western blotting with two different antibodies to examine if the expression level of CENP-F was affected by the F2872A mutation in fibroblasts derived from mutant animals.

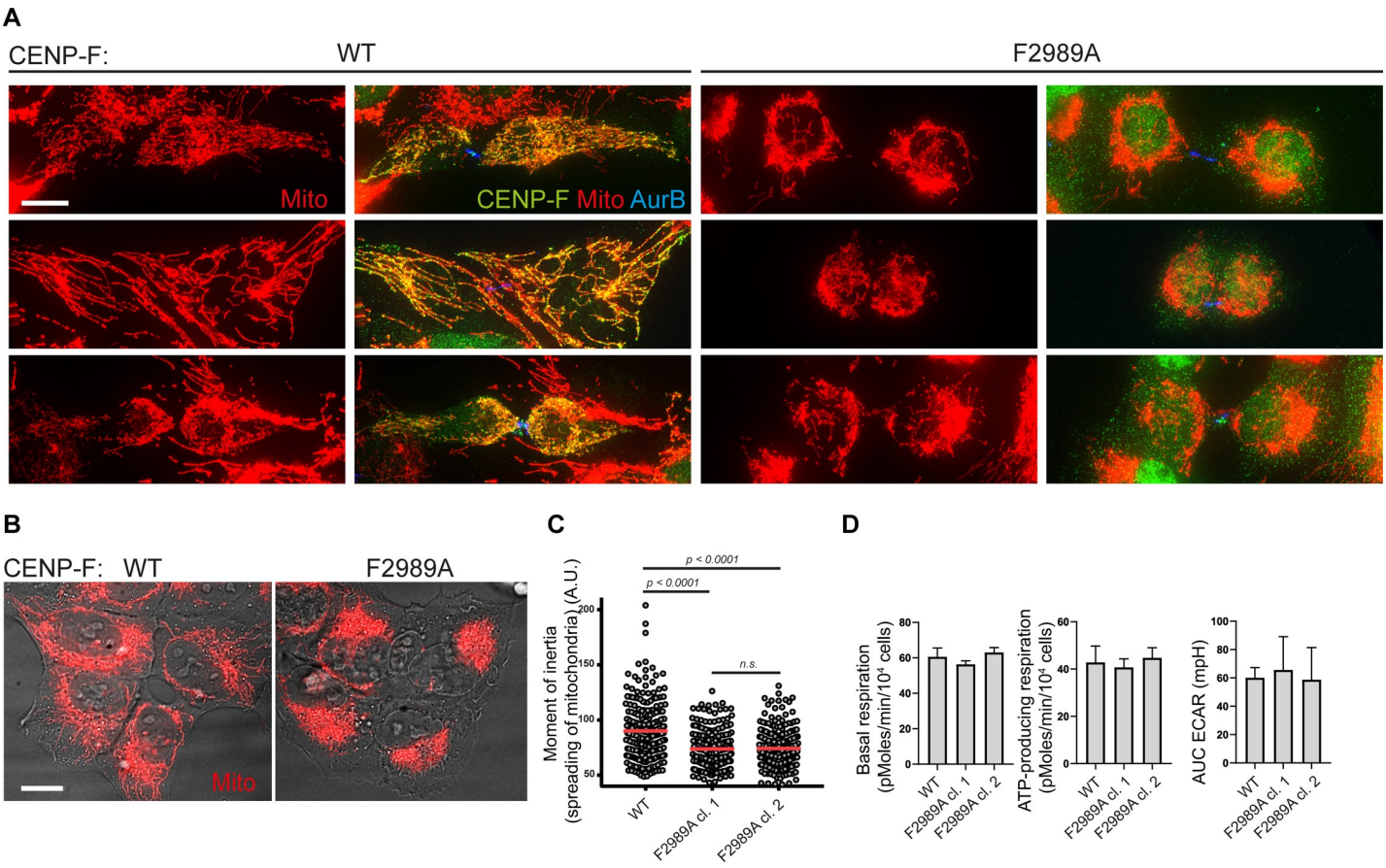

Fig 4. CENP-F-Miro complex is necessary for normal mitochondrial spreading in human cells. A) Immunofluorescence of mtBFP-expressing cytokinetic *CENP-F*^{WT} or *CENP-F*^{F2989A} U2OS cells using a CENP-F antibody (Ab5). **B)** Examples of mitochondrial morphology in live *CENP-F*^{WT} or *CENP-F*^{F2989A} interphase U2OS cells stably expressing mtBFP. **C)** Quantification of the moment of inertia (mitochondrial spreading) of cells exemplified in (B). Significance calculated using Mann-Whitney *U* test (N = at least 228 cells per condition) Two independent *CENP-F*^{F2989A} U2OS clones were used for quantification. **D)** Bioenergetics of U2OS wild type compared to *CENP-F*^{F2989A} mutant as measured by Seahorse analyzer. AUC ECAR = area under curve extracellular acidification rate. Scale bars 5 μm.

https://doi.org/10.1371/journal.pgen.1008050.g004

Using a polyclonal antibody specifically raised against the central area of mouse CENP-F (SCF.M antibody targeting residues 1408–1836. Courtesy of Stephen S. Taylor), we observed comparable expression levels between WT and the F2872A mutant (Fig 5Di). However, contrary to what we observed in the case of the mutant human cells (Fig 2D), we observed a reduced signal for the F2872A point mutant in western blot when using the widely used commercial CENP-F antibody Ab5 (Fig 5Dii). Ab5 is a polyclonal antibody raised against the C-terminal portion of human CENP-F (residues 2760–3114), an area that contains the mutated Miro-binding domain, suggesting that the F2872A mutation disrupts an important epitope. Although raised against the human protein, Ab5 cross-reacts with the mouse protein, owing to the good primary sequence conservation in that area. In fact, the Miro-binding domain is the most conserved region between human and mouse species. The discrepancy between the SCF.M and Ab5 antibodies can therefore be explained as follows: the Ab5 polyclonal antibody preparation might contain antibodies recognizing several epitopes on the human protein, but only a limited set of epitopes on the mouse protein, among which, the Miro-binding domain is a preeminent one. Therefore, we conclude that the F2872A mutation does not affect protein stability but reduces the affinity of the Ab5 antibody for mouse CENP-F.

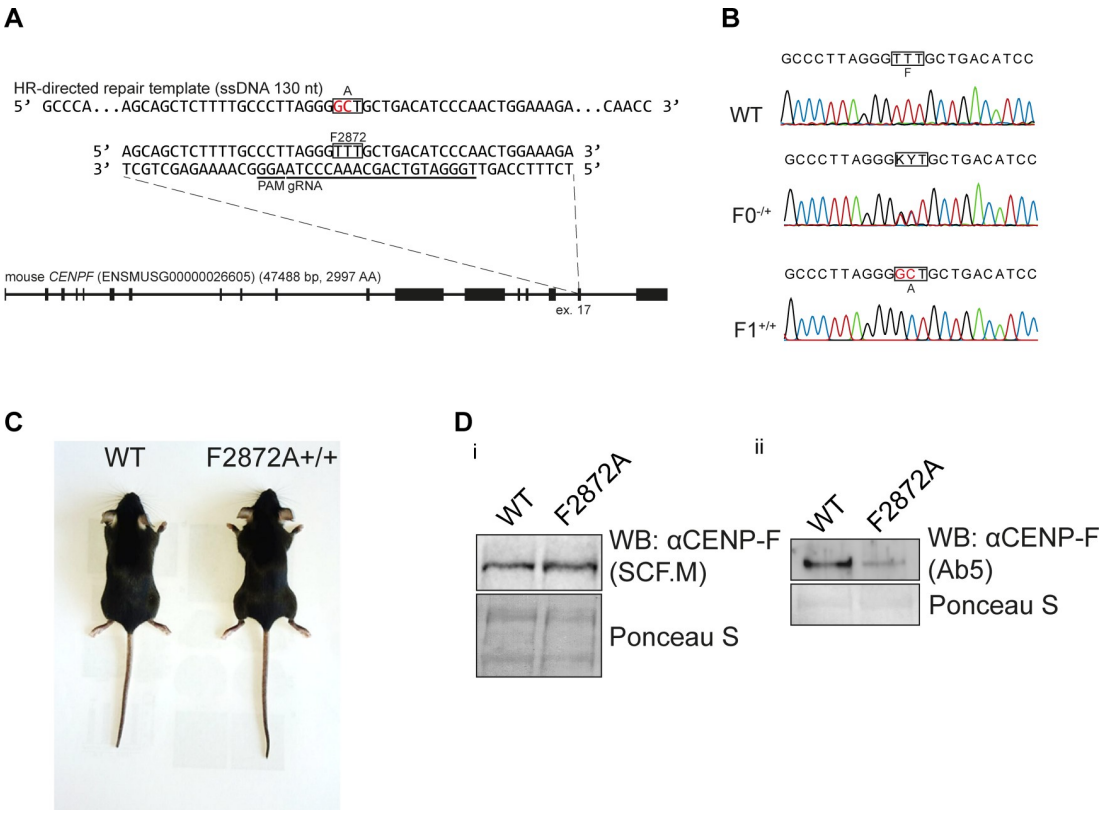

Fig 5. Introduction of the F2872A *CENP-F* mutation in mice. A) Targeting strategy to generate mice carrying *F2872A* in CENP-F using CRISPR/Cas9. **B)** Sequencing electropherograms of the targeted *CENP-F* area from *WT* and *F2872A*-carrying F0 heterozygous or F1 homozygous mice. **C)** 8 weeks old *WT* and homozygous *F2872A* littermate mice **D)** Western blot on primary fibroblasts derived from wild type or *F2872A* mice using i) SCF.M or ii) Ab5 antibody.

https://doi.org/10.1371/journal.pgen.1008050.g005

Since the presence of CENP-F on mitochondria has not been previously demonstrated in mice, we sought to validate the localization of CENP-F in cytokinetic mouse cells using immunofluorescence. The Ab5 antibody that we currently use for CENP-F immunofluorescence in human cells failed to generate a specific signal for murine CENP-F, consistent with a difference in epitopes between mouse and human proteins. We therefore performed all immunofluorescence experiments using the SCF.M antibody. Surprisingly, we did not detect any enrichment of WT CENP-F at mitochondria during cytokinesis in primary mouse fibroblasts (Fig 6A), but another commonly used mouse cell line NMuMG (mammary gland epithelium), displayed characteristic CENP-F enrichment on mitochondria during cytokinesis (Fig 6B). These data suggest that CENP-F-Miro interaction is cell-type specific. To investigate this possibility further, we imaged CENP-F in several cell lines. We found indeed that different cells showed different levels of CENP-F recruitment to mitochondria, with human telomerase-transformed retinal primary epithelial cells (RPE) showing strong recruitment in cytokinesis, while human colorectal carcinoma cells (HCT116) showed no detectable recruitment. Other cancerous (MCF7) or non-cancerous (mouse embryonic stem cells, HEK293) lines showing intermediate levels of recruitment (S1C Fig).

Thus, in order to assess the effect of the F2872A mutation to CENP-F recruitment, we needed to identify primary cells in which CENP-F was robustly recruited to mitochondria. Because NMuMG cells derived from mammary glands displayed evident recruitment (Fig 6B),

Table 1. Heritability of genome-edited *CENP-F* alleles.

	Progeny genotype		
Breeding pair	**% WT**	**% -/+**	**% +/+**
***F2872A*$^{-/+}$ X *F2872A*$^{-/+}$**	24	50	26
***MUT2*$^{-/+}$ X *MUT2*$^{-/+}$**	23	52	25

https://doi.org/10.1371/journal.pgen.1008050.t001

we harvested mammary glands from WT and mutant mice and extracted primary Mouse Mammary Epithelial Cells (MMECs) by digesting the tissue and culturing epithelial mammary gland organoids [36, 37]. Immunofluorescence staining of CENP-F in these cells revealed strong mitochondrial enrichment of CENP-F during cytokinesis in WT cells. On the other hand, no such enrichment was observed in cells derived from *CENP-F*^{F2872A} mutant animals (Fig 6C), indicating that, as in human cells, the F2872 residue was essential for CENP-F-Miro

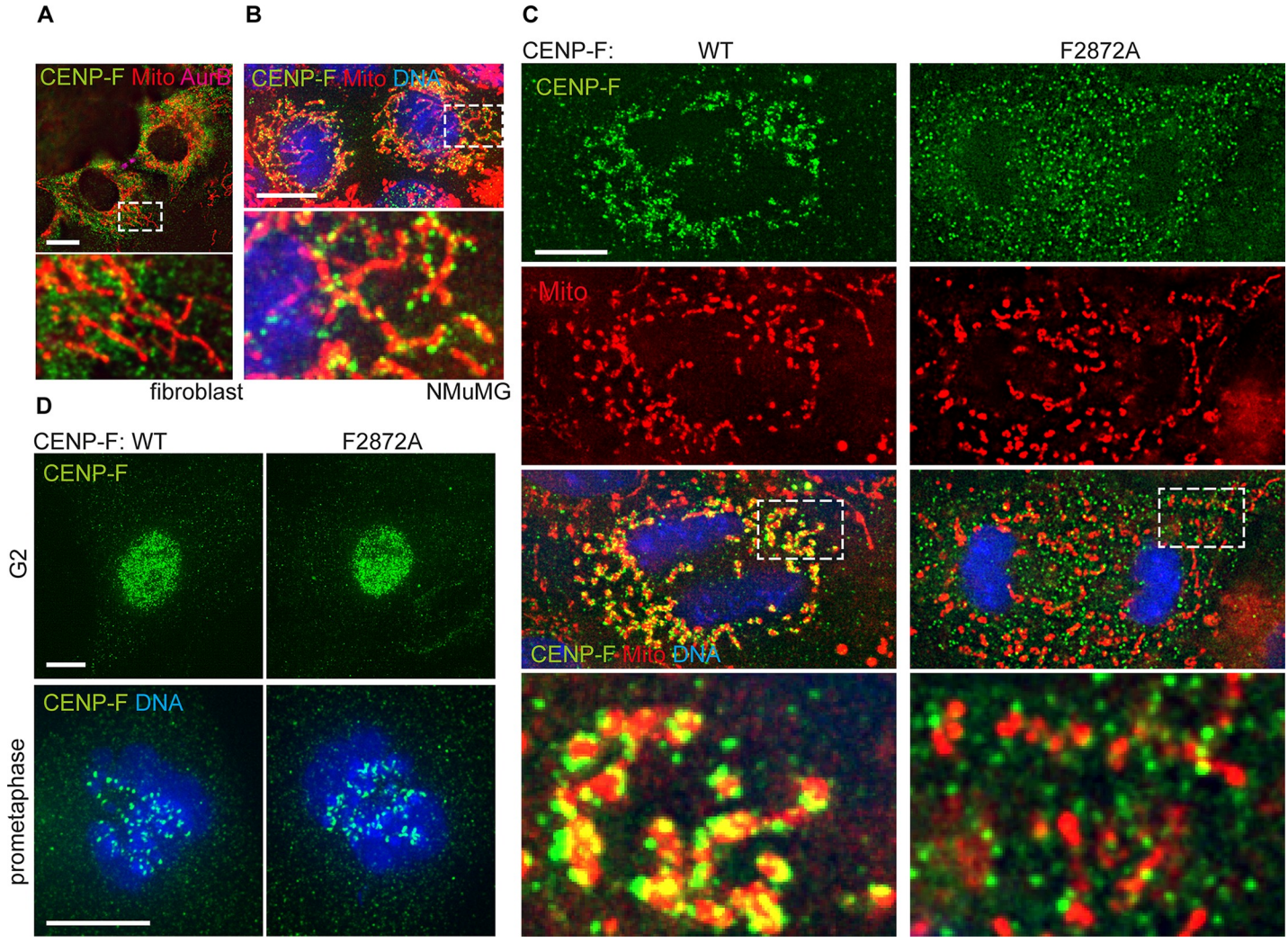

Fig 6. Mitochondrial CENP-F in mice is cell-type specific and can be disrupted by the F2872A mutation. A) Immunofluorescence of mouse fibroblasts stained using CENP-F antibody (SCF.M), Aurora B antibody and mitotracker. **B)** Immunofluorescence of mouse mammary epithelial cell line NMuMG stained using CENP-F antibody (SCF.M), mitotracker and DAPI. **C)** Immunofluorescence of CENP-F (SCF.M antibody) in primary MMECs derived from *WT* or *F2872A* mice and labelled with Mitotracker and DAPI. **D)** Immunofluorescence of CENP-F (SCF.M antibody) in primary MMECs derived from *WT* or *F2872A* mice and labelled with DAPI. Scale bars 5 μm.

interaction in mice. Nevertheless, unlike what was observed in U2OS cells, mitochondria spread equally well to the cell periphery, when compared to WT cells (Fig 6C). This discrepancy might be a consequence of differences in morphology between MMECs and U2OS cells. Unlike U2OS cells, MMECs grow in clusters and remain rounded throughout, and after cytokinesis. Thus, mitochondrial spreading might not require CENP-F in MMECs.

Importantly, as in U2OS cells, CENP-F immunofluorescence revealed that *CENP-F*^{F2872A} is expressed and localized normally as shown by its nuclear accumulation in G2 and distinct kinetochore localization in mitosis (Fig 6D).

Taken together, these results demonstrate cell-type specific mitochondrial recruitment of CENP-F in mice, and show that *CENP-F*^{F2872A} is genetically uncoupled from mitochondria, but retains its other localizations.

As a consequence of homologous recombination being the limiting step in CRISPR knock-in experiments, we obtained two additional alleles that resulted from the repair of the Cas9-induced cuts by non-homologous end joining, in an error-prone manner (all mouse strains created here are summarized in Table 2). The first mutation was a 2bp deletion with a 4bp insertion at the very beginning of exon 17, which resulted in a frameshift starting from residue G2871 (Table 2, Fig 7A, MUT1). The second allele contains a 13bp deletion encompassing the intron 16/exon 17 junction (Table 2, Fig 7A, MUT2). Thus, both of these mutants are expected to yield a truncation of the last two exons, which encode for (1) the C-terminal microtubule-binding domain of CENP-F, (2) part of the Miro-binding domain and (3) the CaaX farnesylation motif. The truncation may also affect the predicted Rb-interaction domain by removing its last five residues [33]. Both of these genotypes resulted in viable homozygous animals that are fertile and reached adulthood without any apparent phenotype (Fig 7B).

We first analyzed the expression levels of the mutant proteins using western blotting on primary fibroblasts. The Ab5 antibody raised against the C-terminus of CENP-F did not detect either allele, confirming that the C-terminus is missing in both mutants (Fig 7C). When using the SCF.M antibody raised against an epitope upstream of the mutations, we observed that both mutants showed reduced CENP-F levels (Fig 7D). This reduction was not caused by nonsense-mediated mRNA decay since quantitative reverse-transcriptase PCR did only detect minor differences in mRNA level between wild type and mutants, even though splicing of intron 16 appeared to be entirely abrogated in Mutant 2 (Fig 7E). We thus conclude that both truncations destabilize CENP-F protein.

MUT2 displayed the most substantial loss of CENP-F expression, prompting us to further analyze the abundance and localization of CENP-F throughout the cell-cycle in these mutant animals. We used Immunofluorescence staining to specifically observe the early mitotic population of cells, which were marked by histone H3 phosphorylation. While late G2/early M-phase WT cells displayed the expected nuclear accumulation of CENP-F, MUT2 cells did not display any CENP-F signal above background levels (Fig 7F). Nevertheless, we could detect residual CENP-F in prometaphase at kinetochores (Fig 7G). This allowed us to quantify the remaining fraction of MUT2 CENP-F by measuring fluorescence intensities of single CENP-F kinetochore foci. The mean fluorescence intensities (a.u.) of 341.5 in WT vs. 68.3 in MUT2 suggest an 80% loss of CENP-F expression in MUT2 (Fig 7H).

Table 2. Mouse lines generated in this study, with description of modified alleles. Numbering of nucleotides and amino acids as in ENSMUSG00000026605.

	DNA	Protein	Strain name
F2872A	g.41109-41110>GC	p.F872A	*cenpf*$^{[p.F872A]BKL}$
MUT1	g.41107-41108>CTCT	p.G2871fsX33	*cenpf*$^{[p.G2871fsX33]BKL}$
MUT2	g.41101del41113	-	*cenpf*$^{[\Delta I/E17]BKL}$

https://doi.org/10.1371/journal.pgen.1008050.t002

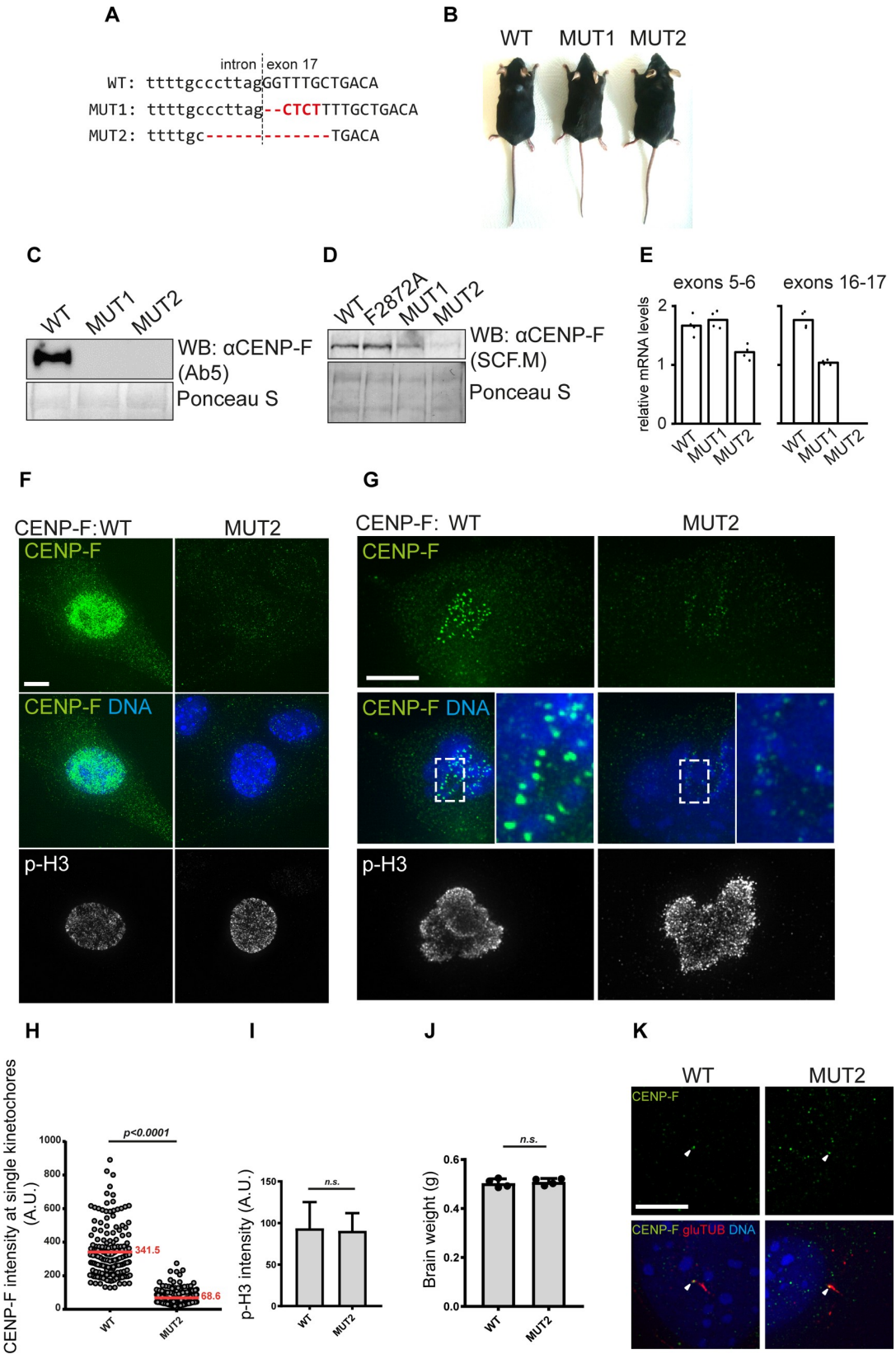
A
intron | exon 17
WT: ttttgcccttagGGTTTGCTGACA
MUT1: ttttgcccttag--CTCTTTTGCTGACA
MUT2: ttttgc------------TGACA
B
WT
MUT1
MUT2
C
WT
MUT1
MUT2
WB: αCENP-F (Ab5)
Ponceau S
D
WT
F2872A
MUT1
MUT2
WB: αCENP-F (SCF.M)
Ponceau S
E
exons 5-6
exons 16-17
relative mRNA levels
WT
MUT1
MUT2
F
CENP-F:WT
MUT2
CENP-F
CENP-F DNA
p-H3
G
CENP-F: WT
MUT2
CENP-F
CENP-F DNA
p-H3
H
CENP-F intensity at single kinetochores (A.U.)
p<0.0001
341.5
68.6
WT
MUT2
I
p-H3 intensity (A.U.)
n.s.
WT
MUT2
J
Brain weight (g)
n.s.
WT
MUT2
K
WT
MUT2
CENP-F
CENP-F gluTUB DNA

Fig 7. Engineering and characterization of CENP-F-truncating mutations in mice. A) CRISPR/Cas9-modified, indel-containing (red) CENP-F alleles in two different mice mutants (MUT1 and MUT2). **B)** Adult WT and homozygous MUT1 and MUT2 mice. **C)** Western blot using Ab5 antibody on primary fibroblasts derived from WT, MUT1 and MUT2 mice. **D)** As in C) but using the SCF.M. antibody. **E)** Relative mRNA levels of CENP-F in wild type and mutant backgrounds assessed by quantitative RT-PCR using primers spanning exons 5 to 6 (left) and 16 to 17 (right). Data are normalized to GAPDH. **F)** Immunofluorescence of late G2 primary fibroblasts from WT and MUT2 mice stained with CENP-F (SCF.M) and p-H3 S10 (06–570) antibodies, DNA labelled with DAPI. **G)** Immunofluorescence of mitotic primary fibroblasts from wild type and MUT2 mice using CENP-F (SCF.M) and p-H3 S10 (06–570) antibodies, DNA labelled with DAPI. **H)** Quantification of kinetochore CENP-F foci intensities in mitotic wild type or MUT2 cells exemplified in (E). At least 160 single kinetochores from 5 individual cells were quantified for each condition. Significance calculated using Mann-Whitney *U* test. Mean values depicted in red. **I)** Mean intensities of p-H3 areas from mitotic cells exemplified in (E). Significance calculated using Mann-Whitney *U* test (N = 5) **J)** Average brain weight of 8 week old WT and MUT2 animals. Significance calculated using Mann-Whitney *U* test (N = 4). **K)** Immunofluorescence of CENP-F and primary cilia (detyrosinated tubulin) in serum starved primary fibroblasts from wild type and MUT2 animals. Scale bars 5 μm.

https://doi.org/10.1371/journal.pgen.1008050.g007

A recent report showed that CENP-F recruits ATR to kinetochores, which leads to activation of the Chk1-Aurora B axis, ultimately resulting in S10 phosphorylation of histone H3 and suppression of chromosome segregation errors [15]. Our analysis did not show any decrease of pH3 S10 in MUT2-derived fibroblasts (Fig 7G and 7I).

Table 3. Oligonucleotides used in this study.

No.	name	5'-3' sequence
1	CenpF_G2988Afwd	GTTGTAAAGAAAGCGTTTGCTGACATC
2	CenpF_G2988Arev	GATGTCAGCAAACGCTTTCTTTACAAC
3	CenpF_F2989Afwd	GTAAAGAAAGGGGCTGCTGACATCCCG
4	CenpF_G2988Arev	GATGTCAGCAAACGCTTTCTTTACAAC
5	CenpF_T2997Afwd	CCGACAGGAAAGGCTAGCCCATATATC
6	CenpF_T2997Arev	GATATATGGGCTAGCCTTTCCTGTCGG
7	hCenpFgRNA8fwd	GAAATTAATACGACTCACTATAGGGGGAT GTCAGCAAACCCTAAGTTTTAGAGCTAGAAATAGC
8	t7gRNAtemprev	AAAAGCACCGACTCGGTGCCACTTTTTCAA GTTGATAACGGACTAGCCTTATTTTAACTTG CTATTTCTAGCTCTAAAAC
9	T7_mcenpf_gRNA7	GAAATTAATACGACTCACTATAGGTGGGATG TCAGCAAACCCTAGTTTTAGAGCTAGAAATAGC
10	dnr_h_gRNA8	ATTATCCTTGTTAAAACCACCTAATGAATATCT TTTCCACTGTAGATAGAATTGGACCTAGCAGT GCTGACAGTTATTTTTTTTGCCCTTAGGGGCT GCTGACATCCCGACAGGAAAGACTAGCCCA
11	cenpf_donor_7	GCCCAGCGAACCCAGCCAAACAGCTAATCAGT GCCATTACCAACAAGCAGCTCTTTTGCCCTTA GGGGCTGCTGACATCCCAACTGGAAAGACAAG CCCATATATCCTTCGGAGAACAACCATGGCAACC
12	h_cf_cas9restr_F	CTGTGTAGTGTTATTTTCCC
13	h_cf_cas9restr_R	GGAGGACTCTGCAAGATTTT
14	cenpfnestfwd	TCTTAGCAAGTGCAGCCT
15	cenpfnestrev	TCTTCACCTTTTGCCCAT
16	CENPF_ex_5-6F	AGTTGAAGAACGGAAGAGGT
17	CENPF_ex_5-6R	TGATGAGGAAGCCTGATGTC
18	CENPF_ex_16-17F	GCCTCCCAGAAGTCGTTAAA
19	CENPF_ex_16-17R	ATGGTTGTTCTCCGAAGGAT
20	mGAPDHfwd2	CATGGCCTTCCGTGTTCCTA
21	mGAPDHrev2	CCTGCTTCACCACCTTCTTGA

https://doi.org/10.1371/journal.pgen.1008050.t003

CENP-F truncation in MUT2 is similar to alleles responsible for Strømme syndrome. A hallmark of Strømme syndrome patients is intestinal atresia, which becomes lethal unless resected. While we did not perform an in-depth phenotypic analysis of MUT2, the normal survival of these mice excludes the presence of intestinal atresia [9, 38]. Moreover, 8 weeks old MUT2 mice showed normal brain weight, suggesting no dramatic microcephaly phenotype, another characteristic of Strømme syndrome patients (Fig 7J). CENP-F was previously shown to localize to the basis of primary cilia [8]. Curious about this localization of the truncated CENP-F, we performed immunofluorescence of CENP-F and detyrosinated tubulin on serum-starved fibroblasts. We detected both the full-length and truncated proteins at the basis of primary cilia, indicating that the C-terminal microtubule-binding domain is not required for this localization (Fig 7K).

Discussion

CENP-F is an enigmatic protein with a plethora of suggested cellular functions ranging from chromosome segregation to mitochondrial trafficking.

Because of the number of its binding partners and involvement in different cellular processes, a careful genetic dissection is needed to study specific roles of CENP-F. Variants of CENP-F have been characterized that separate its functions at the nuclear envelope and kinetochores [12, 14].

Here, we identify a point mutation (F2989A) in the conserved Miro-binding domain of CENP-F, which disrupts its interaction with Miro and thus its ability to be recruited to mitochondria. We thoroughly characterize the behavior of this variant by engineering it in cultured cells, and show that it is completely removed from mitochondria, while retaining other known localizations. To study the physiological relevance of the mitochondrial fraction of CENP-F, we mutated this residue also in mice and validated that CENP-F is removed from mitochondria. Surprisingly, these animals are viable and fertile with no apparent burden.

The transport of mitochondria is a crucial process in long cells like neurons. Its role in non-neuronal cells is much less clear. Preventing CENP-F-Miro interaction causes a drastic defect in mitochondrial spreading in U2OS cells, yet does not prevent the development of apparently healthy and fertile mice. This disconnect between *in vitro* and *in vivo* phenotypes supports a cell-type specific function of CENP-F-mediated mitochondrial trafficking. Indeed, we observe that mouse CENP-F is recruited to mitochondria in a Miro-dependent fashion in primary and immortalized mouse mammary epithelial cells, but not in primary mouse fibroblasts. This suggests that Miro-mediated CENP-F recruitment to mitochondria serves a tissue-specific rather than housekeeping function. What is this function? An in-depth phenotypic analysis of this mouse model is required to answer this question. Since the Miro-binding domain is one of the best conserved features of CENP-F, being almost identical from tunicates to human, it is likely that this function of the Miro-CENP-F interaction is also conserved. What is the molecular basis for the cell-type-specific Miro-CENP-F interaction? CENP-F Miro-binding domain is heavily phosphorylated and contains consensus sequences for several mitotic kinases. It is thus tempting to speculate that differential phosphorylation in different tissues and at different cell-cycle stages promote or inhibit Miro-CENP-F interaction and the subsequent recruitment of CENP-F to the mitochondria.

While the mitochondrial function of CENP-F has been recognized only recently, many conflicting reports exist regarding its function in mitosis. Some studies advocate that CENP-F ensures correct chromosome segregation by regulating kinetochore-microtubule attachments, thus affecting mitotic checkpoint and cell-cycle progression [5, 15–17, 19]. On the contrary, other studies failed to detect any mitotic phenotypes upon CENP-F deletion in HeLa cells [22]

or in mouse fibroblasts [23]. Likewise, the function of the C-terminal farnesylation of CENP-F remains controversial. A number of reports showed diminished CENP-F localization at kinetochores upon farnesyltransferase inhibitor (FTI) treatment or upon mutagenesis of the CaaX motif [28–31]. However, a recent study reported that FTI treatment or mutagenesis of the CaaX motif did not prevent kinetochore localization of CENP-F [32]. Thus, further investigations into the function of CENP-F farnesylation are needed to clarify these conflicting observations.

Here, in addition to the F2872A mutant, we have generated mice carrying CENP-F alleles entirely lacking the C-terminal microtubule binding domain and the farnesylation motif. Both of these have been implicated in possible CENP-F mitotic functions [26, 28]. The normal survival of these animals excludes a drastic global defect in chromosome segregation, but it remains possible that certain cell types might be affected. Importantly, one of the mutated CENP-F alleles displays marked decrease of CENP-F expression. A recent report placed CENP-F as an important activator of mitotic checkpoint at the kinetochore, where it triggers a novel ATR—Chk1—AurB—pH3 pathway. The authors observed decrease in H3 phosphorylation upon expression of a presumed dominant-negative form of CENP-F. We did not see any decrease in H3 phosphorylation in fibroblasts derived from mutant animals. While it is possible that residual CENP-F in MUT2 might be fully capable of ATR activation, our observation is in line with the fact that CENP-F-null MEFs and HeLa cells do not display any defect in chromosome segregation [22, 23], supporting that the mitotic function of CENP-F might be cell type or context specific.

Despite a host of important functions attributed to CENP-F, the protein appears mostly dispensable for mouse development. The most straightforward explanation to this discrepancy lies in the fact that most studies to date have been performed in heavily transformed cancer cell lines. Some of these cell lines might have adapted their kinetochores to the fast pace of their divisions, possibly by becoming heavily dependent on CENP-F. Indeed, CENP-F emerges as a marker that is overexpressed in cancers [7, 39–41]. Here, we find that CENP-F can be downregulated without obvious consequences on animal health. Therefore, inhibiting CENP-F might be a viable avenue for treating CENP-F-dependent cancers.

CENP-F is also involved in human genetic diseases [7–10]. In particular, familial mutations in human CENP-F lead to the Strømme syndrome, a disease characterized by severe ciliopathy phenotypes such as microcephaly and intestinal atresia. Some of the CENP-F mutant alleles found in Strømme patients (e.g. Arg2898*) were shown to cause a decrease in protein levels, perhaps via non-sense mediated decay of the CENP-F message [8]. Interestingly, one of the non-functional CENP-F variants (p.Arg3094) detected in Strømme patients is only predicted to lack the last 20 residues, indicating that minimal perturbations in CENP-F sequence can have drastic effects on human health [9]. Whether such truncation causes decay of CENP-F message is unclear, but since both MUT1 and MUT2 causing larger truncations fail to induce mRNA decay, it is likely that p.Arg3094 also fails to induce decay, unless mouse mRNA metabolism is different from human. We did not find a significant reduction in brain weight in young adult MUT2 animals. However, it should be noted here that mutations in genes causing microcephaly in humans do not cause microcephaly in mice, although microcephaly phenotypes can be recapitulated in other species like ferrets [42]. Nevertheless, the possibility is open that more subtle changes in brain structure might be still present in CENP-F truncated mice. The truncated CENP-F mutant is still present at the base of primary cilia, and although it is not clear whether it retains its cilia-related functionality, this may explain the lack of ciliopathy phenotypes in the mutant mice.

Altogether, the mouse models presented here offer tools to study specifically the physiological functions of the mitochondrial fraction CENP-F, of the C-terminal microtubule-binding

domain including the farnesylation site, and the consequences of global CENP-F downregulation. In the future, it will be important to examine the relevance of these mutants as potential models for CENP-F involvement in Strømme syndrome.

Methods

Sequences

Throughout the manuscript, human CENP-F residues are numbered according to the isoform X1 (Accession number: NP_057427.3), while mouse CENP-F residues are numbered according to the LEK1 sequence (Accession number: Q155P7).

Yeast two-hybrid assay

LexA operator-driven yeast two-hybrid assay was performed as described in [43]. Briefly, bait (pEG202-CENP-F$^{2977\text{-}3020}$) and prey (pJG4-5-Miro1$^{1\text{-}594}$) plasmids were constructed as described previously [4] and transformed into yeast strain EGY48. For the X-gal assay, transformants were plated on Gal/SD-His-Ura-Trp medium and assayed for LacZ reporter induction using the X-gal overlay method [44]. For the growth assay, transformants were plated on Gal/SD-Leu medium and grown for 48hrs at 30˚C. CENP-F alanine point mutants G2988A, F2989A and T2997A were prepared by PCR-based site-directed mutagenesis of the CENP-F bait plasmid using primer pairs 1+2, 3+4 and 5+6 respectively (all primers listed in Table 3). Similarly, to test the interaction between CENP-F and RB, pEG202 bait plasmid expressing CENP-F 2819–3114 fragment and pJG4-5 prey plasmid expressing either full length RB or fragment RB 301–918, were co-expressed in EGY48 yeast strain and the growth was assessed on Leucine dropout medium.

Immunofluorescence

For immunofluorescence staining (IF) using the αCENP-F (Ab5, Abcam), αAuroraB (Clone 6/AIM-1, BD Biosciences) and p-H3 (S10) (Milipore, 06–570) antibodies, cells were grown on coverslips to reach ~80% confluency and fixed using PBS/4% PFA for 30 minutes at room temperature. Subsequently, the samples were washed three times with PBS/0.1% Triton-X100 and incubated in the blocking solution (PBS/10% FCS) for 30 minutes. The samples were then incubated with primary antibodies for 1 hour (dilution 1:300 in blocking solution), washed three times with PBS/0.1% Triton-X100 and incubated with fluorophore-conjugated secondary antibodies (dilution 1:1000 in the blocking solution) for 30 minutes. Finally, the samples were washed three times with PBS/0.1% Triton-X100, three times with PBS and then mounted to slides using Vectashield mounting medium, optionally containing DAPI to visualize DNA. For immunofluorescence staining of mouse cells using SCF.M antibody (kind gift from Stephen Taylor, The University of Manchester), the same steps were performed except that cells were fixed with ice-cold methanol (-20˚C, 10 minutes).To image localization of CENP-F at cilia, primary fibroblasts from wild type and mutant mice were grown to confluency, serum-starved for 8 hours and fixed. Cilia were visualized using antibody against detyrosinated tubulin (AB3201, Sigma, dilution 1:500). To visualize mitochondria when needed, MitoTracker Deep Red FM (Invitrogen/Molecular Probes) was added to the growth media (100nM, 45 minutes) before cell fixation. Imaging was performed using a DeltaVision wide-field microscope (Olympus IX71) equipped with 100x 1.4NA Oil UPlanSApo objective, DAPI-FITC-TRITC-CY5 filter set (Chroma) and Roper CoolSnap HQ2 camera. Images were deconvoluted with Softworx 4.1.0 (Applied Precision). Final image processing and analysis were performed using Fiji [45].

Quantification of mitochondrial spreading

For quantification of mitochondrial spreading, live U2OS cells stably expressing mtBFP [4] were grown and imaged in Labtek chambers. Images of mitochondria were acquired at 37˚C using the wide-field microscope setup described above. For each image of the mitochondrial network, the moment of inertia (equivalent of mitochondrial spreading) was calculated using custom Fiji and Matlab scripts as detailed previously [4].

Respiration measurements

Basal respiration, ATP-linked respiration and extracellular acidification rate (ECAR) of U2OS wild type and U2OS CENP-F^{F2989A} were measured using the Seahorse XF analyzer according to manufacturer instructions. Briefly, cells were plated to a Seahorse XF24 (Agilent) cell culture microplate and grown to near-confluency. For each treatment, 5 wells were used. Basal respiration was determined in XF base medium (Agilent) containing 25 mM glucose, 1 mM pyruvate and 2mM l-glutamine. ATP-linked respiration and ECAR were measured after addition of oligomycin (1μM final concentration). Non-mitochondrial respiration was measured after addition of antimycin A (1μM final concentration). Results were analyzed using the Seahorse XF software and normalized to the number of cells.

Quantification of CENP-F kinetochore localization and p-H3 signal intensity

To quantify residual CENP-F at kinetochores, CENP-F MUT2 and WT mitotic fibroblasts were fixed and labelled using the SCF.M αCENP-F antibody, and DAPI to visualize mitotic chromosomes. Z-sections of prometaphase cells were acquired in 0.3 μM steps using the wide-field microscope described above and then deconvoluted. Images were subsequently processed and analyzed in Fiji. In short, the sections were Z-projected (maximum intensity) and kinetochore CENP-F signal was calculated using the *IntDen—(Area * Mean)* formula (*IntDen* = integrated signal density of a single kinetochore, *Area* = the size of the selected kinetochore area and *Mean* = the mean fluorescence of the CENP-F signal outside the kinetochores). At least 164 single kinetochores were measured for each condition. To quantify phosphorylation of histone H3 phosphorylation in mitotic cells, MUT2 and WT fibroblasts were immunostained for p-H3 (S10) and processed similarly. Mean fluorescence intensities of p-H3 (S10) areas in mitotic cells were measured and normalized to the background.

Western blotting

Primary skin fibroblasts or U2OS cells were harvested and lysed in 8M urea with 3% SDS. Equal amounts of protein lysates as measured by the Bradford assay (Bio-Rad) were resolved by SDS-PAGE and analyzed by western blotting using Ab5 or SCF.M antibodies (1:500 dilution).

Generation of CRISPR/Cas9-edited U2OS cells

CENP-F was targeted using electroporation (Neon system, Invitrogen) of Cas9 RNPs and DNA template for homologous recombination (also see Fig 2 for strategy details). Briefly, ~200.000 cells were harvested, washed with PBS and resuspended in 5 μl of Neon R buffer (Invitrogen). Shortly before electroporation, Cas9 RNP mix (100 pmol of Cas9 (NLS-Cas9, a kind gift from Martin Jinek, University of Zurich), 120 pmol of sgRNA and 200 pmol of single stranded donor DNA template (10, Table 2) in total volume of 5 μl of Neon R buffer) was added to the cell suspension and electroporation was performed using 10 μl Neon tips with

electroporation parameters set to 1400V, 15 ms, and 4 pulses. Immediately after electroporation, cells were seeded into 0.5 ml of pre-warmed growth medium and grown for 3 days. Cells were then single-cloned and colonies arising from single clones were used for PCR amplification of the targeted *CENP-F* locus using primers 12+13. The resulting PCR product was sequenced using primer 12 or digested by TseI to screen for the intended modification (Fig 2B). Clones containing homozygous F2989A mutations in *CENP-F* were collected for further analysis.

Generation of CRISPR/Cas9-edited CENP-F mutant mice

Mice were generated and all animal work was performed in the animal facility of ETH Zurich (EPIC) according to the Swiss Federal Veterinary Office (BVET) guidelines. Animals were regularly checked for potential burden.

CENP-F knock-in and truncated alleles in mice (B6D2F1 x C57Bl/6NTac mixed background) were generated using a modified Cas9-RNPs approach [46]. gRNA sequence targeting the proximity of the CENP-F F2872 codon was selected using the CRISPR design tool (http://crispr.mit.edu/) (also see Fig 5A for details of the targeting strategy). *In vitro* transcribed sgRNA was prepared as described below. ssDNA containing F2872A codon change flanked by 60nt homology arms was used as a template for homologous recombination (11, Table 2). Injection mix was assembled on ice by mixing 200 nM of Cas9-NLS (NEB), 400 nM sgRNA and 100 ng/μl ssDNA donor in the injection buffer (8 mM Tris-HCl, pH 7.4, 0.1 mM EDTA). The mix was injected into pronuclei of fertilized single-cell embryos using standard microinjection procedures. Injected embryos were re-implanted into foster mothers. The pups were genotyped by PCR on genomic DNA extracted from ear clips using primers 14+15. The resulting PCR product was sequenced using primer 14.

In vitro transcription of sgRNAs

sgRNAs were prepared using MEGAshortscript T7 Transcription Kit and MEGAclear Transcription Clean-Up Kit (Ambion) according to manufacturer instructions. The DNA template for *in vitro* transcription was generated by PCR-assembly of partially overlapping oligonucleotides containing T7 promoter sequence, mouse or human CENP-F gRNA target sequence (Figs 2A and 5A) and an invariant Cas9 scaffold sequence (human: primers 7+8, mouse: primers 9+8).

Primary mouse cells isolation

Primary skin fibroblasts were isolated as described step-by-step in [47]. In brief, approximately $1cm^2$ of skin was collected from the underarm area of freshly euthanized ~ 8-week-old animals, cut into small pieces and dissociated in 10ml of Liberase TL (Roche) solution (0.14 Wunsch units/mL in DMEM/F12 + 1X antibiotic/antimycotic) at 37˚C for 1 hour while stirring. Dissociated tissue fragments were collected by centrifugation (520g/5 minutes) and washed three times in DMEM/F12 with 15% FBS to remove remaining Liberase. The tissue fragments were then plated in DMEM/F12 with 15% FBS + 1X antibiotic/antimycotic and grown at 37˚C, 5% CO_2 for 7 days allowing fibroblasts to exit the tissue.

Mouse mammary epithelial cells (MMECs) were isolated as described in [36, 37]. In brief, 3^{rd}, 4^{th} and 5^{th} pairs of mammary glands were collected from freshly euthanized ~ 8-week-old animals, minced using scissors and dissociated in Collagenase A (Roche) solution (2 mg/ml in DMEM/F12 + 1X antibiotic/antimycotic) at 37˚C for 2 hours while stirring. The dissociated epithelial organoids were pelleted from the suspension by centrifugation (250g/5 minutes) and resuspended in 5ml DMEM/F12. The organoids were again pelleted (250g/5 minutes) and

resuspended in 10ml PBS/5% FBS. The pellet was then resuspended and washed with 10ml PBS/5% FBS five times (400g/15 seconds) to remove single cells from the organoids. After the last washing step, the pellet containing pure epithelial organoids was resuspended in DMEM/F12, 10% FBS, 5 μg/ml insulin (Sigma, I0516), 1 μg/ml hydrocortisone (Sigma, H0888), 5 ng/ml hEGF (Sigma, E9644) + 1X PSG mix) for 48 hours and switched to serum-reduced medium (DMEM/F12, 5% FBS, 5 μg/ml insulin, 1 μg/ml hydrocortisone, 5 ng/ml EGF + 1X PSG mix) to prevent growth of remaining fibroblasts. Epithelial cells escaped the organoids within 2–3 days and were immediately processed for immunofluorescent staining.

RNA quantification. Total RNA was extracted from livers of 8 week old animals using TRIzol (Invitrogen) according to manufacturer's instructions. Reverse transcription of 2 μg of total RNA was performed using SuperScript III reverse transcriptase (Invitrogen) according to manufacturer's instructions. Resulting cDNA was analyzed with LightCycler 480 II (Roche) using SYBR green master mix (Roche) according to manufacturer instructions. CENP-F specific primers and GAPDH internal control primers used to normalize results are listed in Table 3.

Ethics statement. Mice were generated and all animal work was performed in the animal facility of ETH Zurich (EPIC) in strict accordance with the Schweizerisches Tierschutzgesetz (Animal Welfare Act), the subordinate Tierschutzordnung (Animal Welfare Ordinance) and Tierversuchsverordnung (Animal Experimentation Ordinance), and approved by the Swiss Federal Veterinary Office (BVET). Animals were regularly checked for potential burden.

Supporting information

S1 Fig. A) Yeast-two-hybrid assay between the region of CENP-F encompassing the presumed RB-binding domain and full length or fragment 301–918 of RB, fails to yield any positive signal, as assessed by the growth on medium lacking Leucine. By contrast, the same fragment of CENP-F yields robust interaction signal with Miro1. **B)** Western blotting of yeast extracts showing that both full-length and 301–918 fragments of RB are well expressed. Since the interaction between RB and CENP-F is deemed to be direct, and since fragments of both proteins have been successfully used in two-hybrid assays, it appears that the interaction between RB and CENP-F is weak. **C)** Immunofluorescence of different cell lines stained using CENP-F SCF.M or CENP-F Ab5, Aurora B, mitotracker and DAPI. **D)** Immunofluorescence of mtBFP-expressing cytokinetic *CENP-F*^{WT} or *CENP-F*^{F2989A} U2OS cells using a CENP-F antibody (Ab5). Scale bars 5 μm.
(TIF)

S1 File. Source data for Fig 4C and 4D, and Fig 7E, 7H–7J.
(XLSX)

Acknowledgments

We are grateful to the EPIC facility of ETH Zurich & Thomas Hennek for help with generating and handling CRISPR-edited mice, Martin Jinek (University of Zurich) for kindly providing recombinant Cas9 and Stephen S. Taylor (The University of Manchester) for kindly sharing the SCF.M antibody. We thank Andrea Aloia and Werner Kovacs (ETH Zurich) for support with the Seahorse measurements. We also thank all members of the Kornmann lab for providing comments on the manuscript. Microscopy was performed at the Scientific Center for Optical and Electron Microscopy of the ETH Zurich.

Author Contributions

Conceptualization: Martin Peterka, Benoît Kornmann.

Funding acquisition: Benoît Kornmann.

Investigation: Martin Peterka.

Methodology: Martin Peterka.

Project administration: Benoît Kornmann.

Writing – original draft: Martin Peterka, Benoît Kornmann.

Writing – review & editing: Martin Peterka, Benoît Kornmann.

References

1. Rattner JB, Rao A, Fritzler MJ, Valencia DW, Yen TJ. CENP-F is a .ca 400 kDa kinetochore protein that exhibits a cell-cycle dependent localization. Cell motility and the cytoskeleton. 1993; 26(3):214–26. https://doi.org/10.1002/cm.970260305 PMID: 7904902.
2. Ma L, Zhao X, Zhu X. Mitosin/CENP-F in mitosis, transcriptional control, and differentiation. Journal of Biomedical Science. 2006; 13(2):205–13. https://doi.org/10.1007/s11373-005-9057-3 PMID: 16456711
3. Varis A, Salmela A-L, Kallio MJ. Cenp-F (mitosin) is more than a mitotic marker. Chromosoma. 2006; 115(4):288–95. https://doi.org/10.1007/s00412-005-0046-0 PMID: 16565862
4. Kanfer G, Courtheoux T, Peterka M, Meier S, Soste M, Melnik A, et al. Mitotic redistribution of the mitochondrial network by Miro and Cenp-F. Nat Commun. 2015; 6. ARTN 8015 https://doi.org/10.1038/ncomms9015 WOS:000360351600007. PMID: 26259702
5. Feng J, Huang H, Yen TJ. CENP-F is a novel microtubule-binding protein that is essential for kinetochore attachments and affects the duration of the mitotic checkpoint delay. Chromosoma. 2006; 115 (4):320–9. https://doi.org/10.1007/s00412-006-0049-5 WOS:000238497400005. PMID: 16601978
6. Dees E, Miller PM, Moynihan KL, Pooley RD, Hunt RP, Galindo CL, et al. Cardiac-specific deletion of the microtubule-binding protein CENP-F causes dilated cardiomyopathy. Disease models & mechanisms. 2012; 5(4):468–80. Epub 2012/05/09. https://doi.org/10.1242/dmm.008680 PMID: 22563055; PubMed Central PMCID: PMCPMC3380710.
7. Aytes A, Mitrofanova A, Lefebvre C, Alvarez Mariano J, Castillo-Martin M, Zheng T, et al. Cross-Species Regulatory Network Analysis Identifies a Synergistic Interaction between FOXM1 and CENPF that Drives Prostate Cancer Malignancy. Cancer Cell. 2014; 25(5):638–51. https://doi.org/10.1016/j.ccr.2014.03.017 PMID: 24823640
8. Waters AM, Asfahani R, Carroll P, Bicknell L, Lescai F, Bright A, et al. The kinetochore protein, CENPF, is mutated in human ciliopathy and microcephaly phenotypes. Journal of medical genetics. 2015; 52 (3):147–56. Epub 2015/01/08. https://doi.org/10.1136/jmedgenet-2014-102691 PMID: 25564561; PubMed Central PMCID: PMCPMC4345935.
9. Filges I, Bruder E, Brandal K, Meier S, Undlien DE, Waage TR, et al. Stromme Syndrome Is a Ciliary Disorder Caused by Mutations in CENPF. Human mutation. 2016; 37(4):359–63. Epub 2016/01/29. https://doi.org/10.1002/humu.22960 PMID: 26820108.
10. Ozkinay F, Atik T, Isik E, Gormez Z, Sagiroglu M, Sahin OA, et al. A further family of Stromme syndrome carrying CENPF mutation. American journal of medical genetics Part A. 2017; 173(6):1668–72. Epub 2017/04/14. https://doi.org/10.1002/ajmg.a.38173 PMID: 28407396.
11. Bolhy S, Bouhlel I, Dultz E, Nayak T, Zuccolo M, Gatti X, et al. A Nup133-dependent NPC-anchored network tethers centrosomes to the nuclear envelope in prophase. The Journal of cell biology. 2011; 192 (5):855–71. Epub 2011/03/09. https://doi.org/10.1083/jcb.201007118 PMID: 21383080; PubMed Central PMCID: PMCPMC3051818.
12. Berto A, Yu J, Morchoisne-Bolhy S, Bertipaglia C, Vallee R, Dumont J, et al. Disentangling the molecular determinants for Cenp-F localization to nuclear pores and kinetochores. EMBO reports. 2018; 19(5). https://doi.org/10.15252/embr.201744742 PMID: 29632243
13. Ciossani G, Overlack K, Petrovic A, Huis In 't Veld PJ, Koerner C, Wohlgemuth S, et al. The kinetochore proteins CENP-E and CENP-F directly and specifically interact with distinct BUB mitotic checkpoint Ser/Thr kinases. The Journal of biological chemistry. 2018; 293(26):10084–101. Epub 2018/05/12. https://doi.org/10.1074/jbc.RA118.003154 PMID: 29748388; PubMed Central PMCID: PMCPMC6028960.

14. Zhu X. Structural requirements and dynamics of mitosin-kinetochore interaction in M phase. Molecular and cellular biology. 1999; 19(2):1016–24. Epub 1999/01/16. https://doi.org/10.1128/MCB.19.2.1016 PMID: 9891037; PubMed Central PMCID: PMCPMC116032.

15. Kabeche L, Nguyen HD, Buisson R, Zou L. A mitosis-specific and R loop–driven ATR pathway promotes faithful chromosome segregation. Science. 2017. https://doi.org/10.1126/science.aan6490 PMID: 29170278

16. Bomont P, Maddox P, Shah JV, Desai AB, Cleveland DW. Unstable microtubule capture at kinetochores depleted of the centromere-associated protein CENP-F. The EMBO Journal. 2005; 24 (22):3927–39. https://doi.org/10.1038/sj.emboj.7600848 PMID: 16252009

17. Holt SV, Vergnolle MAS, Hussein D, Wozniak MJ, Allan VJ, Taylor SS. Silencing Cenp-F weakens centromeric cohesion, prevents chromosome alignment and activates the spindle checkpoint. Journal of Cell Science. 2005; 118(20):4889–900. https://doi.org/10.1242/jcs.02614 PMID: 16219694

18. Laoukili J, Kooistra MR, Bras A, Kauw J, Kerkhoven RM, Morrison A, et al. FoxM1 is required for execution of the mitotic programme and chromosome stability. Nature cell biology. 2005; 7(2):126–36. Epub 2005/01/18. https://doi.org/10.1038/ncb1217 PMID: 15654331.

19. Yang Z, Guo J, Chen Q, Ding C, Du J, Zhu X. Silencing mitosin induces misaligned chromosomes, premature chromosome decondensation before anaphase onset, and mitotic cell death. Molecular and cellular biology. 2005; 25(10):4062–74. https://doi.org/10.1128/MCB.25.10.4062-4074.2005 PMID: 15870278; PubMed Central PMCID: PMC1087709.

20. Evans HJ, Edwards L, Goodwin RL. Conserved C-terminal domains of mCenp-F (LEK1) regulate subcellular localization and mitotic checkpoint delay. Experimental cell research. 2007; 313(11):2427–37. Epub 2007/05/15. https://doi.org/10.1016/j.yexcr.2007.03.035 PMID: 17498689; PubMed Central PMCID: PMCPMC3991481.

21. Vergnolle MAS, Taylor SS. Cenp-F links kinetochores to Ndel1/Nde1/Lis1/Dynein microtubule motor complexes. Curr Biol. 2007; 17(13):1173–9. https://doi.org/10.1016/j.cub.2007.05.077 WOS:000247852100031. PMID: 17600710

22. McKinley KL, Cheeseman IM. Large-Scale Analysis of CRISPR/Cas9 Cell-Cycle Knockouts Reveals the Diversity of p53-Dependent Responses to Cell-Cycle Defects. Developmental Cell. 2017; 40 (4):405–20.e2. https://doi.org/10.1016/j.devcel.2017.01.012 PMID: 28216383

23. Pfaltzgraff ER, Roth GM, Miller PM, Gintzig AG, Ohi R, Bader DM, et al. Loss of CENP-F results in distinct microtubule-related defects without chromosomal abnormalities. Molecular Biology of the Cell. 2016; 27(13):1990–9. https://doi.org/10.1091/mbc.E15-12-0848 PMID: 27146114

24. Raaijmakers JA, van Heesbeen, Blomen VA, Janssen LME, van Diemen F, Brummelkamp TR, et al. BUB1 Is Essential for the Viability of Human Cells in which the Spindle Assembly Checkpoint Is Compromised. Cell Reports. 2018; 22(6):1424–38. https://doi.org/10.1016/j.celrep.2018.01.034 PMID: 29425499

25. Kanfer G, Peterka M, Arzhanik VK, Drobyshev AL, Ataullakhanov FI, Volkov VA, et al. CENP-F couples cargo to growing and shortening microtubule ends. Molecular Biology of the Cell. 2017; 28(18):2400–9. https://doi.org/10.1091/mbc.E16-11-0756 WOS:000408693800006. PMID: 28701340

26. Volkov VA, Grissom PM, Arzhanik VK, Zaytsev AV, Renganathan K, McClure-Begley T, et al. Centromere protein F includes two sites that couple efficiently to depolymerizing microtubules. The Journal of cell biology. 2015; 209(6):813–28. Epub 2015/06/24. https://doi.org/10.1083/jcb.201408083 PMID: 26101217; PubMed Central PMCID: PMCPMC4477864.

27. Ashar HR, James L, Gray K, Carr D, Black S, Armstrong L, et al. Farnesyl transferase inhibitors block the farnesylation of CENP-E and CENP-F and alter the association of CENP-E with the microtubules. The Journal of biological chemistry. 2000; 275(39):30451–7. https://doi.org/10.1074/jbc.M003469200 PMID: 10852915.

28. Hussein D, Taylor SS. Farnesylation of Cenp-F is required for G2/M progression and degradation after mitosis. J Cell Sci. 2002; 115(Pt 17):3403–14. PMID: 12154071.

29. Schafer-Hales K, Iaconelli J, Snyder JP, Prussia A, Nettles JH, El-Naggar A, et al. Farnesyl transferase inhibitors impair chromosomal maintenance in cell lines and human tumors by compromising CENP-E and CENP-F function. Molecular cancer therapeutics. 2007; 6(4):1317–28. https://doi.org/10.1158/1535-7163.MCT-06-0703 PMID: 17431110.

30. Gurden MD, Holland AJ, van Zon W, Tighe A, Vergnolle MA, Andres DA, et al. Cdc20 is required for the post-anaphase, KEN-dependent degradation of centromere protein F. J Cell Sci. 2010; 123(Pt 3):321–30. Epub 2010/01/08. https://doi.org/10.1242/jcs.062075 PMID: 20053638; PubMed Central PMCID: PMCPMC2816182.

31. Holland AJ, Reis RM, Niessen S, Pereira C, Andres DA, Spielmann HP, et al. Preventing farnesylation of the dynein adaptor Spindly contributes to the mitotic defects caused by farnesyltransferase inhibitors.

Mol Biol Cell. 2015; 26(10):1845–56. https://doi.org/10.1091/mbc.E14-11-1560 PMID: 25808490; PubMed Central PMCID: PMCPMC4436830.

32. Moudgil DK, Westcott N, Famulski JK, Patel K, Macdonald D, Hang H, et al. A novel role of farnesylation in targeting a mitotic checkpoint protein, human Spindly, to kinetochores. The Journal of cell biology. 2015; 208(7):881–96. https://doi.org/10.1083/jcb.201412085 PMID: 25825516; PubMed Central PMCID: PMCPMC4384735.

33. Ashe M, Pabon-Pena L, Dees E, Price KL, Bader D. LEK1 is a potential inhibitor of pocket protein-mediated cellular processes. The Journal of biological chemistry. 2004; 279(1):664–76. Epub 2003/10/14. https://doi.org/10.1074/jbc.M308810200 PMID: 14555653.

34. Yang M, Wu Z, Fields S. Protein-peptide interactions analyzed with the yeast two-hybrid system. Nucleic acids research. 1995; 23(7):1152–6. PMID: 7739893.

35. Janssen A, Medema RH. Genetic instability: tipping the balance. Oncogene. 2012; 32:4459. https://doi.org/10.1038/onc.2012.576 PMID: 23246960

36. McCaffrey LM, Macara IG. The Par3/aPKC interaction is essential for end bud remodeling and progenitor differentiation during mammary gland morphogenesis. Genes & development. 2009; 23(12):1450–60. Epub 2009/06/17. https://doi.org/10.1101/gad.1795909 PMID: 19528321; PubMed Central PMCID: PMCPMC2701573.

37. Karantza-Wadsworth V, White E. A Mouse Mammary Epithelial Cell Model to Identify Molecular Mechanisms Regulating Breast Cancer Progression. Methods in enzymology. 2008; 446:61–76. https://doi.org/10.1016/S0076-6879(08)01604-2 PMC2857708. PMID: 18603116

38. Gao N, White P, Kaestner KH. Establishment of intestinal identity and epithelial-mesenchymal signaling by Cdx2. Dev Cell. 2009; 16(4):588–99. Epub 2009/04/24. https://doi.org/10.1016/j.devcel.2009.02.010 PMID: 19386267; PubMed Central PMCID: PMCPMC2673200.

39. O'Brien SL, Fagan A, Fox EJ, Millikan RC, Culhane AC, Brennan DJ, et al. CENP-F expression is associated with poor prognosis and chromosomal instability in patients with primary breast cancer. International journal of cancer. 2007; 120(7):1434–43. Epub 2007/01/06. https://doi.org/10.1002/ijc.22413 PMID: 17205517; PubMed Central PMCID: PMCPMC4972098.

40. Zhuo YJ, Xi M, Wan YP, Hua W, Liu YL, Wan S, et al. Enhanced expression of centromere protein F predicts clinical progression and prognosis in patients with prostate cancer. Int J Mol Med. 2015; 35 (4):966–72. https://doi.org/10.3892/ijmm.2015.2086 WOS:000351764800014. PMID: 25647485

41. Falagan S, Vlagea A, Moreno-Rubio J, Casado E, Sereno M. A retrospective analysis of the correlation between anti-CENP-F titres and malignant tumors. Journal of Clinical Oncology. 2018; 36(15_suppl): e13565–e. https://doi.org/10.1200/JCO.2018.36.15_suppl.e13565

42. Johnson MB, Sun XS, Kodani A, Borges-Monroy R, Girskis KM, Ryu SC, et al. Aspm knockout ferret reveals an evolutionary mechanism governing cerebral cortical size. Nature. 2018; 556(7701):370–+. https://doi.org/10.1038/s41586-018-0035-0 WOS:000430285200050. PMID: 29643508

43. Golemis EA, Serebriiskii I, Finley RL Jr., Kolonin MG, Gyuris J, Brent R. Interaction trap/two-hybrid system to identify interacting proteins. Current protocols in cell biology. 2011;Chapter 17:Unit 17.3. Epub 2011/12/14. https://doi.org/10.1002/0471143030.cb1703s53 PMID: 22161546.

44. Serebriiskii IG, Golemis EA. Uses of lacZ to study gene function: evaluation of beta-galactosidase assays employed in the yeast two-hybrid system. Analytical biochemistry. 2000; 285(1):1–15. Epub 2000/09/22. https://doi.org/10.1006/abio.2000.4672 PMID: 10998258.

45. Schindelin J, Arganda-Carreras I, Frise E, Kaynig V, Longair M, Pietzsch T, et al. Fiji: an open-source platform for biological-image analysis. Nature methods. 2012; 9(7):676–82. Epub 2012/06/30. https://doi.org/10.1038/nmeth.2019 PMID: 22743772; PubMed Central PMCID: PMCPMC3855844.

46. Sung YH, Kim JM, Kim HT, Lee J, Jeon J, Jin Y, et al. Highly efficient gene knockout in mice and zebrafish with RNA-guided endonucleases. Genome research. 2014; 24(1):125–31. Epub 2013/11/21. https://doi.org/10.1101/gr.163394.113 PMID: 24253447; PubMed Central PMCID: PMCPMC3875853.

47. Seluanov A, Vaidya A, Gorbunova V. Establishing Primary Adult Fibroblast Cultures From Rodents. Journal of Visualized Experiments: JoVE. 2010;(44):2033. https://doi.org/10.3791/2033 PMC3185624. PMID: 20972406